EFFECTS OF URBANIZATION AND KANIV RESERVOIR ON THE THERMAL CHARACTERISTICS IN THE REGION

MIROSLAV PIKL[1], OLGA BROVKINA[1,*], FRANTIŠEK ZEMEK[1,3], MARYNA LADYKA[2], and VLADIMIR STARODUBTSEV[2]

[1] Global Change Research Institute of the Czech Academy of Sciences, Brno, Bělidla 4a, 603 00, Czech Republic
[2] National University of Life and Environmental Sciences of Ukraine, Heroyiv Oborony st., 15, Kyiv, 03041, Ukraine
[3] University of South Bohemia in České Budějovice, Faculty of Agriculture and Technology, Branišovská 1645/31a, České Budějovice, 370 05, Czech Republic
* Corresponding author: brovkina.o@czechglobe.cz

ABSTRACT

This study contributes to understanding the effects of urbanization and a large body of water, Kaniv Reservoir, on thermal characteristics in the region. This was done by recording trends in air and surface temperatures in the growing seasons in the period 1985–2022. Specifically, the study's objectives were to 1) detect and quantify changes in built-up areas using Landsat satellite data, and 2) analyse trends in land surface temperature (LST) in several shoreland zones of the reservoir with different land covers. To identify built-up areas, Landsat data was processed. LST was calculated using Google Earth Engine for the period studied for three shoreland zones and six types of land cover, including sites with substantial, partial and no change in land use. The built-up area increased unevenly over time and differently in each of the shoreland zones. The growth in built-up area was greatest, increasing by 3.7 times, in a zone close to the city of Kyiv. The highest mean LST values were recorded in the zone that was mainly agricultural. Positive LST trends were recorded throughout the entire period of the study, albeit with different trend slopes in individual months. Statistically significant trends were recorded only in August and September.

Keywords: built-up area; land surface temperature; land cover change; satellite remote sensing; regional

Introduction

Kaniv Reservoir, also known as Kaniv Hydroelectric Power Plant Reservoir, is a large body of water in central Ukraine and the second reservoir in the Dnipro Cascade. It was established in the 1970s by the construction of the Kaniv Dam on the Dnipro River. Construction of the Kaniv Dam and the reservoir's creation had significant effects on the surrounding area.

Recent studies (Starodubtsev et al. 2021; Vyshnevskyi and Shecvhuk 2021) report the spatiotemporal dynamics of this hydromorphic landscape, shoreland erosion, overgrowing of the reservoir with vegetation, and other ecological aspects related to development in and around Kaniv Reservoir. In wet years flood water is released from the reservoir through culverts into low-lying areas adjacent to the reservoir. The capacity of the low-lying areas was sufficient to hold the flood water even in very wet years. Urbanization and development in the low-lying areas greatly reduced this capacity. For this reason, Kaniv Reservoir in the future may not be able to prevent the flooding in vast areas of the southern part of the city of Kyiv. Knowledge of the changes in the urban land cover in the low-lying areas around the shores of Kaniv Reservoir might be helpful in estimating actual capacity of the whole area to hold flood water in very wet years. Moreover, it potentially could account for some of the ecological and anthropogenic changes that have occurred in recent years, namely the newly built-up areas close to the reservoir. This study reports the changes in land cover and reflected changes in land surface temperature (LST) in shoreland zones and neighbouring regions of the Kaniv Reservoir. This was done using satellite data that are available for almost the entire period of the reservoir's operation, recent field observations and standardized maps.

There are two maps of land cover known to the authors that include the shoreland zones around the Kaniv Reservoir. The first is that for Ukraine for 1990, 2000 and 2010 with a 30-meter spatial resolution (Kussul et al. 2016). This map includes a neural network classification of satellite Landsat images that identifies six classes of land cover within the European Land Use and Cover Area Frame Survey (LUCAS) nomenclature: artificial surfaces, cropland, grassland, forest, bare land, and water. The second is GlobeLand30, which consists of global land cover maps for 2000, 2010 and 2020 with a 30-meter spatial resolution (Chen et al. 2014). The maps include images from the Landsat satellite and HJ-1 (China Environment and Disaster Reduction Satellite) that identify 10 land cover classes: namely cultivated land, forest, grassland, shrubland, wetland, bodies of water, tundra, artificial surfaces, bare land and perennial snow and ice. Artificial surfaces in these two maps differ in their accuracy because of the different methods used. The layers have slightly different definitions and include several types of artificial objects, such as settlements, mining areas, transportation facilities and so forth, whereas the current study is focused on the increase in built-up areas at the local level. Also, these two maps do not cover the period at the start of the operation of Kaniv Reservoir. The changes in urban area throughout the entire period of the operation of this reservoir have not so far been studied.

Pikl, M., Brovkina, O., Zemek, F., Ladyka, M., Starodubtsev, V.: Effects of urbanization and Kaniv Reservoir on the thermal characteristics in the region
European Journal of Environmental Sciences, Vol. 14, No. 1, pp. 33–42
https://doi.org/10.14712/23361964.2024.4

Land surface temperature (LST) is an important component of the Earth's energy budget and is increasingly used in various applications related to the assessment of land surface conditions, including mapping the urban extent (Trlica et al. 2017; Bala et al. 2021; He et al. 2021) and the nature of urban microclimates (Li et al. 2020a). The Landsat satellite time series can be used to provide LST estimates at high spatial resolutions, which are particularly appropriate for local and small-scale studies. Google Earth Engine (GEE) (Gorelick et al. 2017) is an online platform created for users of remote sensing to carry out big data analyses in a user-friendly manner and without the need for computation.

Changes in urban area, among other factors, can potentially influence the thermal regime of the shoreland zones of a reservoir (Dawson et al. 2018). Human pressure resulting from urbanization, is one of the main factors leading to increasing risk to shorelands, bearing in mind future climate change scenarios. The recent study of Arulbalaji et al. (2020) reports a marked increase in built-up area and in mean LST in a coastal town in India during the period of their study. The temperature in built-up areas is higher than in the surroundings even in a shoreland zone with abundant vegetation (Tarawally et al. 2018).

In recent decades, the water temperature in the Dnipro Cascade increased in summer by 0.74 °C per decade and during May–October by 0.65 °C per decade (Vyshnevskyi and Shecvhuk 2021). Apart from the effects of climatic factors, the temperature of the water in the Kaniv Reservoir is influenced by the fact that the reservoir discharges water from its lower layers, where the processes of heating and cooling are very slow. During spring and summer, water temperature recorded in the upper zone of the Kaniv Reservoir is lower than that recorded in the surroundings and in autumn it is higher. The temperature of the water in Kaniv Reservoir also depends on the intensity of algal blooms, with higher temperatures recorded in areas where there are large blooms.

This study aims to improve the level of understanding of the effect of ongoing land use/cover changes and a large water reservoir on the thermal characteristics of different land use/cover types in the region and to identify the trends in surface temperature recorded during the growth seasons in the period 1985–2022. In particular, the objectives were to 1) detect and quantify changes in built-up areas using Landsat satellite data and 2) analyse trends in surface temperatures in several shoreland zones around the reservoir and at sites with different types of land cover.

Materials and Methods

Area studied

Kaniv Reservoir is one of six water reservoirs on the Dnipro River. Construction of the Kaniv Dam began in 1963 and the reservoir began to be filled in 1972. Filling to the normal water level (NWL) was completed in 1976. Kaniv is classified as a large dam (Obodovskyi 2002). The area of the water surface at NWL 91.5 m is 581 km^2 and the volume is 2.62 km^3. At the level dead storage (LDS) 91.0 m, the volume is 2.20 km^3. The so-called "working" volume between NWL and LDS is 0.30 km^3. Length of the reservoir is 123 km, maximum width is 8 km, mean width is 5.5 km, mean depth is 3.9 m and maximum depth is 21 m (Vyshnevskyi et al. 2011).

Kaniv Reservoir's maximum operating level (MOL), also termed full supply level, is 92.7 m (Decree of Ministry of Environmental Protection and Natural Resources of Ukraine, 2022). This water level and ASTER digital elevation model (NASA/METI/AIST/Japan Spacesystems and US/Japan ASTER Science Team 2019) were used to define the area of interest, delineated as the area that would be flooded when water in the dam reaches MOL (Fig. 1). Based on local expert knowledge about the processes prevailing in certain parts of the water body and nearby shore, the area of interest was divided into 3 zones:

Zone_1 is located adjacent to the city of Kyiv. It is undergoing intensive construction and expansion of infrastructure, mainly residential and personal recreation in nature. Water covers approximately 25% of the area and there are islands of alluvial vegetation. In contrast, *Zone_2* is predominantly covered by open water, accounting for about 50% of the area. It also includes an army-expropriated territory with long-term disturbed soil and vegetation cover, making up around 15% of the total area. *Zone_3* is a flat area with no direct contact with the water reservoir. It is mainly an agricultural area where

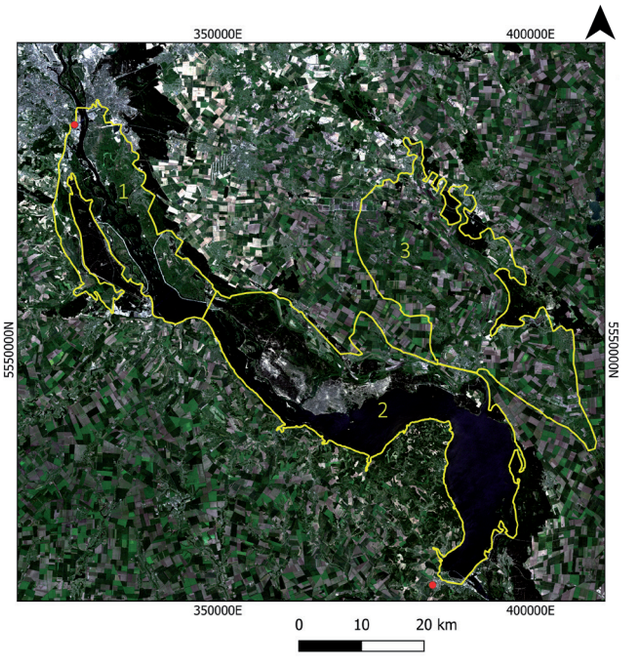

Fig. 1 Photograph of the general area with the three areas studied (1, 2 and 3) demarcated by yellow lines. Red points are the locations of the Kyiv (north) and Kaniv (south) meteorological stations.

crops of winter wheat, corn, sunflower, soybean, winter rapeseed, barley and sugar beet are grown between scattered villages and small towns.

The region has a moderately cold climate, classified as Dfb (**warm-summer humid continental climate**) (Köppen 1936). Precipitation is substantial, even in the driest month and amounts to 677 mm per year. The mean annual temperature is 9.0 °C (Martazinova 2019). The growth period starts in May and ends in September.

Data

Satellite data

Multispectral satellite Landsat (NASA) data for the years 1985, 2000 and 2022 were used to analyse changes in built-up area (Table 1).

Table 1 Satellite data used to analyse changes in built-up area.

Data	Date	Processing level	Source
Landsat-5	6 June 1985	Surface reflectance, L2A	https://earthexplorer.usgs.gov/
Landsat-7	7 June 2000		
Landsat-9	20 June 2022		

Land surface temperature

LST values were estimated using the Statistical Mono-Window algorithm developed by the Climate Monitoring Satellite Application Facility and the GEE online platform (Ermida et al. 2020), which enables large amounts of satellite thermal time-series data to be analysed. The program code returns mean LST value for an object (shape file) and date specified by the user. The number of available mean LST values derived from Landsat data for each zone or site varied between months and hence also between years because of different zone or site locations, layout of acquired satellite data and cloudiness. In the analyses, only those LST values for the same date for all zones and sites were used. The LSTs for the three zones and six small sites with different types of land cover in Zone 1 were recorded. The six small sites are places where there have been dramatic changes in land use, with one land cover type being replaced by another (e.g., vegetation to built-up area), places where there have been partial changes within a land cover, and places without any land use change (Table 2), (Fig. 2). LST values were obtained for available dates from May to September for 1985 to 2022. The code of Ermida et al. (2020) was complemented with *ee.Reducer.count* procedure to count the

Table 2 Land cover types at six small sites (S1–S6) in Zone 1 for 1985, 2000 and 2022.

	S1	S2	S3	S4	S5	S6
1985	fields	vegetation	forest	built-up area	vegetation with built-up areas	water
2000	fields	vegetation with built-up areas	forest	built-up areas	built-up areas	water
2022	fields	built-up areas	forest	built-up areas	built-up areas	water

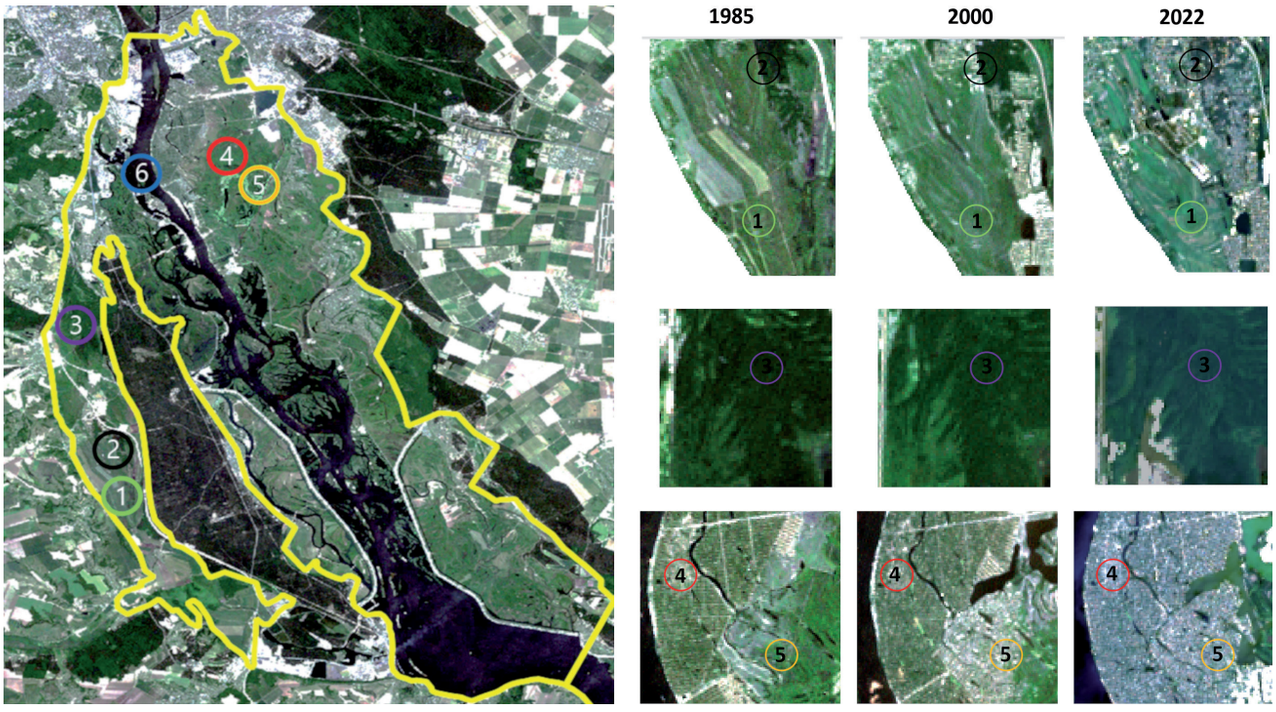

Fig. 2 Small sites used in the analysis of changes in surface temperature for the period 1985–2022: (1) site where there was no change in land use (agricultural), (2) site where there was great change (vegetation to built-up area), (3) and (4) sites where there was no change (forest and built-up area, respectively), (5) site with small changes (sparsely built-up area to densely built-up area) and (6) site where there was no change (water).

number of valid pixels (i.e., without clouds and shadows) for each location and each date involved in calculating mean LSTs. The LST data (Landsat 4, 5, 7, 8, 9) was sorted for each location and each date, and the values used were those with more than 75% valid pixels.

Climate data

Air temperature data was provided by the Central Geophysical Observatory of Ukraine (http://cgo-sreznevskyi.kyiv.ua/?lang=en) from the Kyiv and Kaniv meteorological stations. The daily mean air temperatures were used to analyse the difference between the Kyiv and Kaniv measurements, and 9:30 a.m. air temperature for Kyiv based on the analysis of Landsat LST. The dates of the air temperature records are the same as the dates of the LSTs obtained from satellite Landsat imagery using the GEE algorithm.

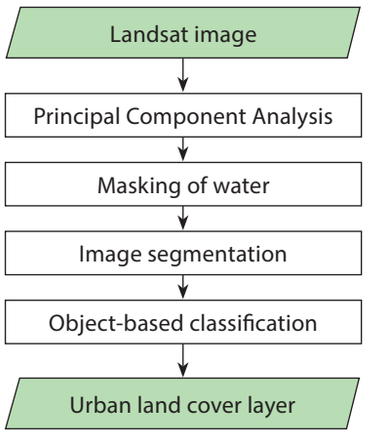

Fig. 3 Main steps in the processing of Landsat data.

Processing of Landsat satellite data

To identify built-up areas, the same steps were used for the classification of Landsat-5, Landsat-7 and Landsat-9 data so that the classification results are comparable (Fig. 3).

The principal component analysis (PCA, also referred to as "PC transform") of the Landsat-5 and Landsat-9 scenes was used to remove redundant information from the dataset while retaining as much of the original spectral information as possible. This resulted in a set of uncorrelated image bands, termed *PC_bands* or components (Chuvieco 2016). The explained variance indicated how much of the total variation in the original data is included in each component. Generally, the first few components of the PCA correspond to dominant features, whereas the later components may represent noise or subtle variations. The first two *PC_bands* from Landsat data PCA analysis accounted for 93.4% of the total variance and were used in subsequent analyses.

Significant parts of Zone 1 and Zone 2 and was covered with water and were not included in the urban land cover classification. PCA_band_1 was used to remove water from each Landsat scene with thresholds, $9450 \leq \text{PCA\_band\_1} \leq 10090$.

Fig. 4 Photographs of the Kaniv Reservoir shoreland zone landscapes (2021).

Segmentation was used to divide an image into segments of similar spectral and/or textural characteristics. The spectral and textural attributes were computed for each band of the input image (two *PC_bands* from Landsat image PCA). The value of the spectral attribute for a particular segment was computed from the input data band where the segmentation label image had the same value (ENVI Reference Guide). The spectral attributes include mean, maximum, minimum, and standard deviation values for the pixels in the image of the region in each band. Computation of the textural attribute was a two-step process wherein the first applied a square kernel of predefined size to the input image. The textural attributes were calculated in terms of pixels in the kernel window (7 × 7 pixels) and the result was referenced to the central kernel. Next, mean values of the attribute results were calculated for each pixel in the segment to create the attribute value for that band's segmentation label. The textural attributes consisted of the range, mean, variance and entropy of the pixels in the kernel. The watershed transform algorithm (Roerdink and Meijster 2001) with scale level of 50 and merge level of 80 was used for the image segmentation.

Training regions for built-up areas for supervised object-based classification were selected using archival and current high-resolution satellite imagery (visualization in Google Earth) and photographs taken in the field in 2021 and 2022 (Fig. 4). Overall, 52 training regions were selected from Landsat scene 1985, 106 from Landsat scene 2000 and 156 from Landsat scene 2022.

The object-based classification was done using the K Nearest neighbour algorithm (Cover and Hart 1967) with a threshold value of 5%, meaning that segments having a less than 5% confidence in each class were set to "unclassified." The overall accuracy and kappa coefficient were used to estimate the classification results.

Statistical analysis of air temperature data and land surface temperature

Analysis of air temperature data and land surface temperature was done using the Statistica (StatSoft) software TIBCO Data Science (https://www.statistica.com/en/). One-way ANOVA was used to test for significant differences among the LST of zones where there was no water cover in months or years during the growth season. A simple linear regression model was used to estimate the LST for each month during the growth season for the six cover classes.

Results

Changes recorded in built-up areas from 1985 to 2022

The accuracy of the estimate of the built-up area based on kappa coefficients for 1985, 2000 and 2022, respectively, were 80% and 0.82, 78% and 0.82 and 82% and 0.84.

The built-up area increased from 1985 to 2022 (Fig. 5). This increase was uneven over time, however, and different in each of the three zones (Table 3, Fig. 6). Built-up

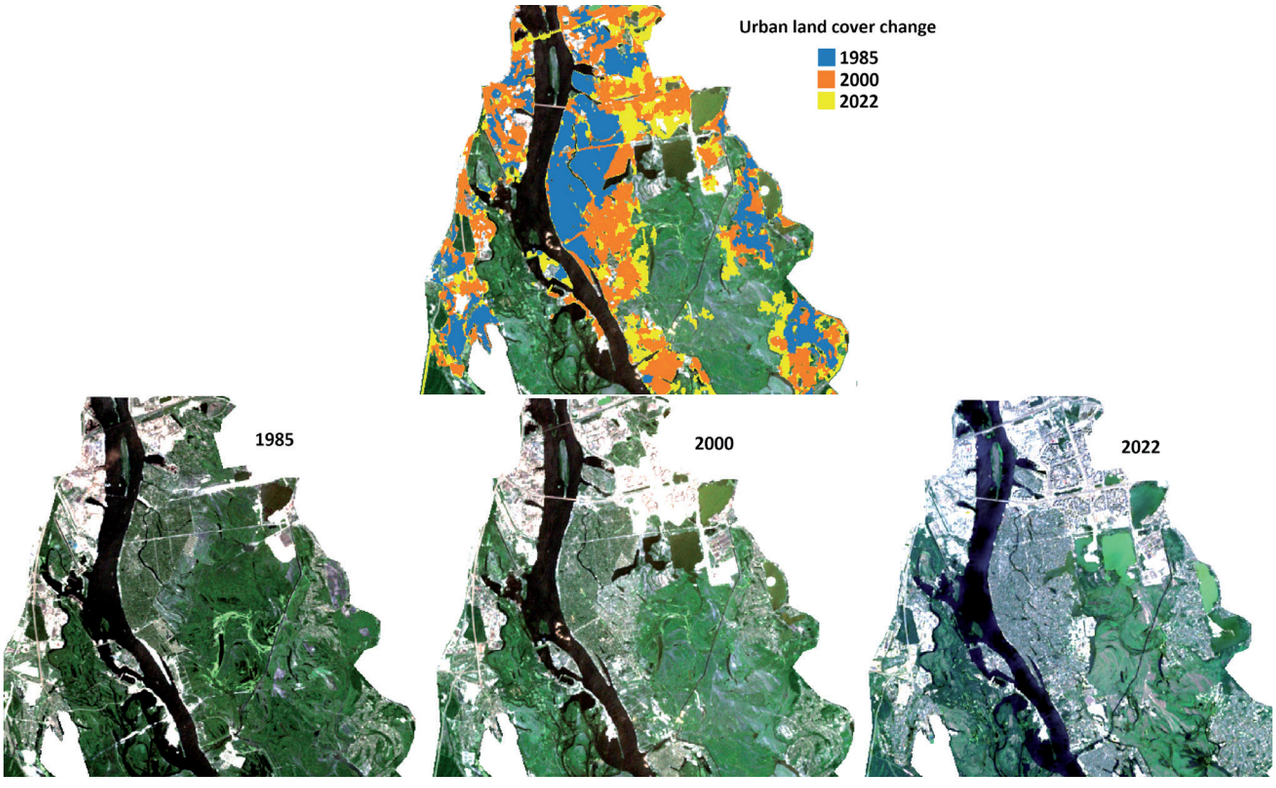

Fig. 5 Part of the map showing the change in the area built-up (at the top) and Landsat scenes (at the bottom).

area increased by 3.7 times in Zone 1, and approximately doubled in zones 2 and 3 from 1985 to 2022.

Table 3 Built-up area recorded in zones 1, 2 and 3 of the area studied in 1985, 2000 and 2022.

Zone	1985	2000	2022
1	24.81 km^2	56.18 km^2	93.40 km^2
2	13.66 km^2	20.38 km^2	29.75 km^2
3	43.75 km^2	57.93 km^2	84.41 km^2
Total	82.22 km^2	134.49 km^2	207.56 km^2

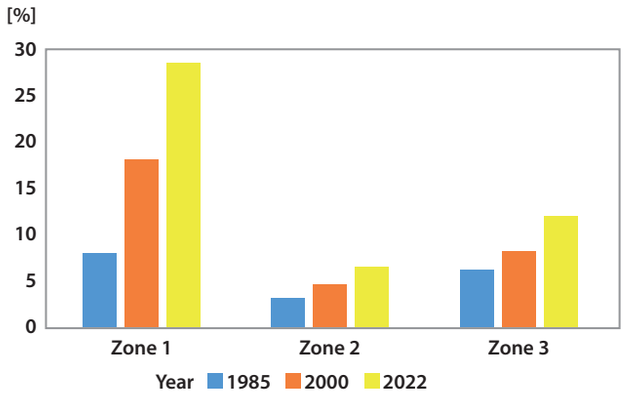

Fig. 6 Changes in the built-up area recorded in zones 1, 2 and 3 of the area studied in 1985, 2000 and 2022. The built-up area is a percentage of the total land area in each zone (areas of water were excluded from the analysis).

Trends in the temperature of the air and surface of the land

Based on the trend in the daily mean air temperature recorded by the Kyiv and Kaniv meteorological stations, the temperature increased by approximately 4 degrees over a period of 37 years (Fig. 7).

LST patterns for zones 1, 2 and 3 without water followed that of the air temperature (Fig. 8a). Zone 3 nearly had the highest LST values for each month from May to September compared to other zones, followed by Zone 2 and Zone 1, both of which lack open water. There was a significant difference ($p < 0.01$) between Zone 3 and the other two zones in mean LST for the months of May and September. Moreover, Zone 3 reached its LST peak throughout summer while both Zone 2 and Zone 3 had a prominent peak in July, which coincided with the peak in air temperature. A similar trend in LST occurred in the yearly means for the growth season. This development followed an evenly increasing trend until 2002, after which the trends for all zones, including air temperature, were very variable (Fig. 8b).

The objective was to determine if the trend in LST is common to all the small sites and therefor attributable to climate change or if the trend in LST differed and is attributable to changes in land cover and/or use (Fig. 9). There are two months, namely August and September, for which the trends (regression coefficients) are similar and statistically significant ($p < 0.01$) and differences in LST values for different classes can be attributed to type of surface cover. There were not statistically significant ($p > 0.05$) trends in LST for other months and classes or for air temperature. For additional information (regression coefficients) see Appendix.

Discussion

The largest increase in built-up area over the period 1985 to 2022 occurred in Zone 1 (3.7 times increase) from 1985 to 2022 (Fig. 6). This may be due to its closeness to the city of Kyiv, the growing interest of the population in life outside the city, and, therefore, intensive construction and expansion of infrastructure. Built-up area in zones 2 and 3 approximately doubled. This can be accounted for by the growth in the rural population within the Boryspil Raion during the period of this study (Timonina 2020).

The accuracy of estimate of the area built-up in this study is less than in other recent publications based on satellite data. The accuracy of the dataset for this study was limited by that of the Landsat satellite data, as the interest in this study was in changes in built-up area since

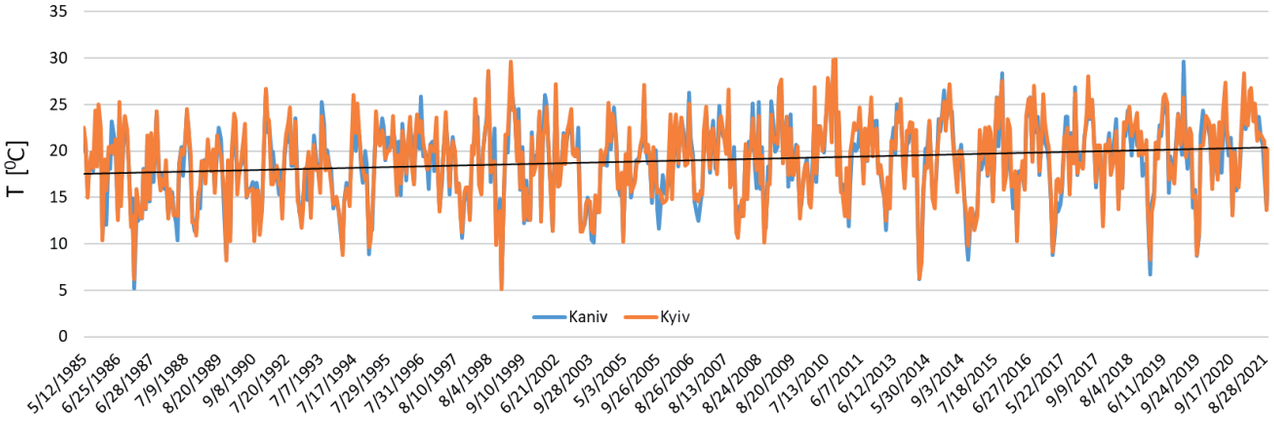

Fig. 7 Daily mean air temperature recorded by the Kaniv and Kyiv meteorological stations over the 37year period from 1985 to 2022.

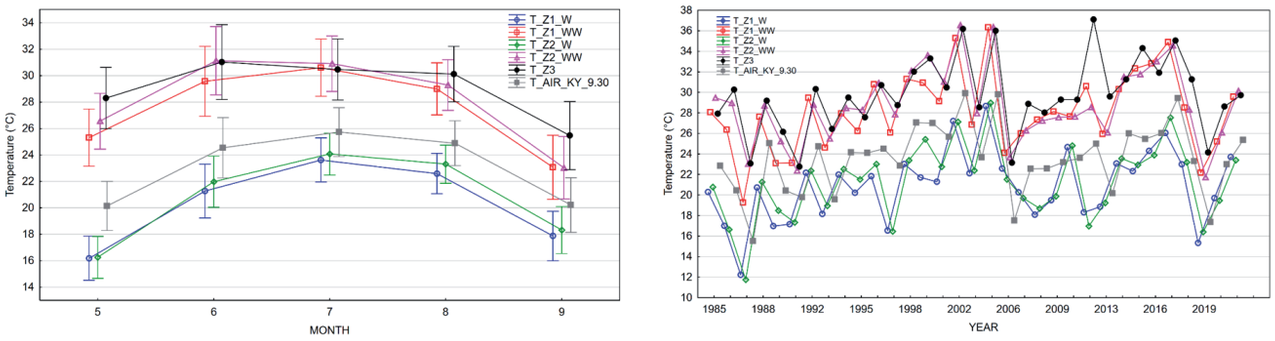

a) b)

Fig. 8 Mean land surface temperature (LST) for the months May through to September (a) and (b) for the period of 37 years for zones with open water (T_Z1_W, T_Z2_W) and without open water (T_Z1_WW, T_Z2_WW, T_Z3) together with air temperature (T_Air_KY_9.30).

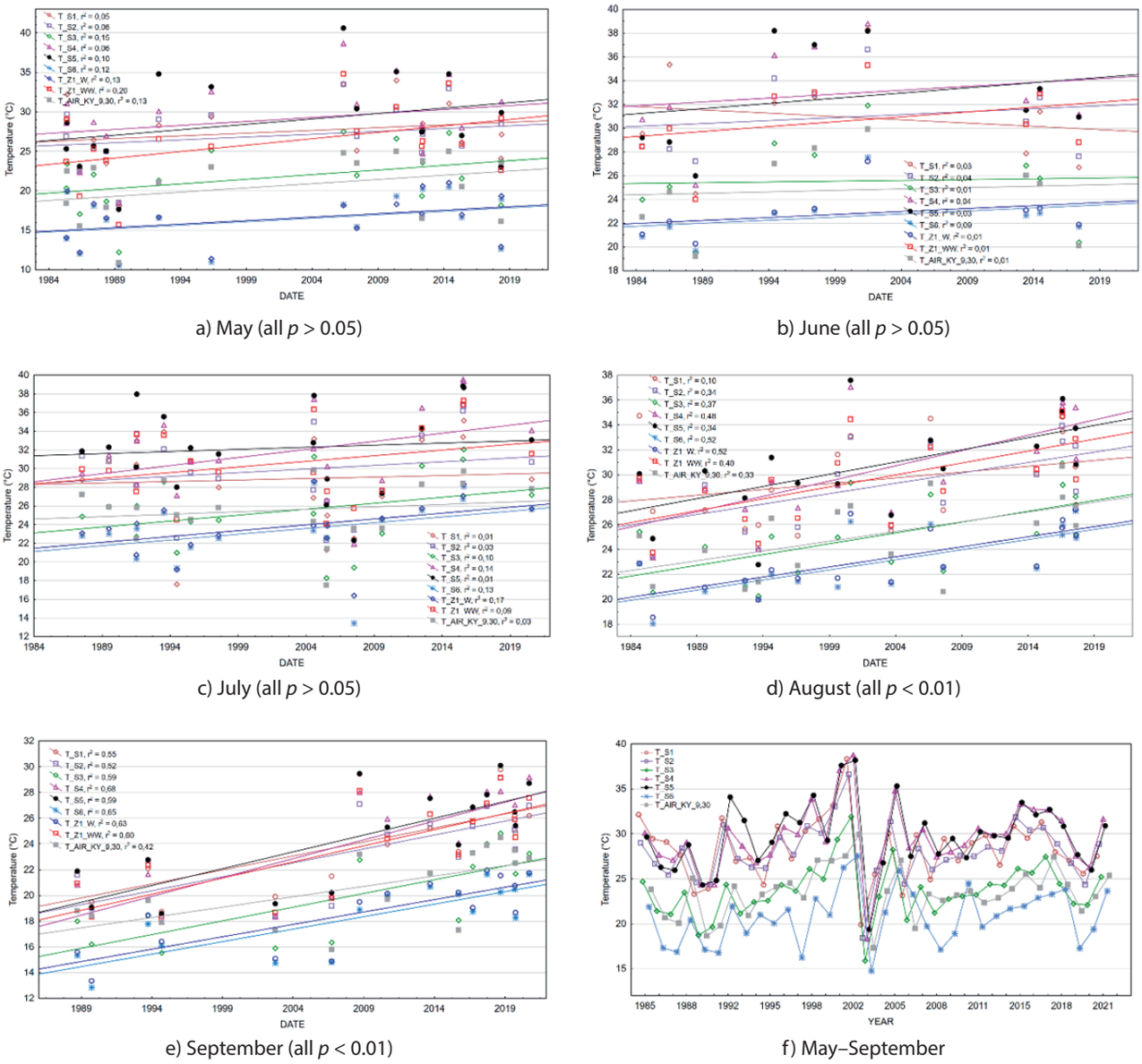

a) May (all $p > 0.05$)

b) June (all $p > 0.05$)

c) July (all $p > 0.05$)

d) August (all $p < 0.01$)

e) September (all $p < 0.01$)

f) May–September

Fig. 9 Trend in surface temperature for the period 1985–2022. (a)–(e) individual months from May to September and (f) all months. The graphs are for six small sites (T_S1–T_S6) in Zone 1 (T_Z1), with an area of reservoir water (T_Z1_W), without an area of reservoir water (T_Z1_WW) and air temperatures for Kyiv (T_AIR_KY_9.30).

the beginning of the operation of the water reservoir in the 1970s to 2022 calculated using the same algorithm and source of satellite data. Whereas the recent publications mentioned below use a single land use classification and/or combined Landsat satellite data with other imagery, which accounts for the slightly higher classification accuracy compared to that of this study. Kussul et al. (2016) report an overall accuracy of classification for the whole of Ukraine in 2010 of about 89% using an unsupervised neural network algorithm for Landsat-8 and Sentinel-1 satellite data. Prasomsup et al. (2020) using a Modified Built-Up Index based Landsat-8 data reports an 82–83% accuracy for the estimates of the built-up areas in Bangkok.

The higher LST values for Zone 3 compared with the other zones for each month from May to September (Fig. 8a) can be accounted for in the remoteness of Zone 3 from the water reservoir, lack of inland water and agriculture, which dominates almost the entire zone. Agricultural fields can create microclimates in their surroundings. Fields with bare soil or sparse vegetation have a higher LST because of their low evapotranspiration compared to fields with dense vegetation. Morsy and Aboelkhair (2021) report that the relative effect of agriculture on LST in Egypt (calculated as the ratio between the change in each area and the sum of all changes in all areas multiplied by the change in LST or normalized difference vegetation index) was 45%, followed only by deserts with an effect of 50%. According to Vendrov et al. (1968) and Kurbanov and Kurbanov (2014), the direct influence of water reservoirs on the microclimate of nearby areas extends for distances of several hundred meters and in the direction of the wind it can be up to 10 km. Zone 3 was about 14 km from the Kaniv Reservoir.

Zone 1 had the greatest growth in built-up area throughout the entire study and it was expected that it would have the highest LST. Being on the bank of the reservoir, the LST of Zone 1 was affected this body of water. The LST of built-up areas combined with the water's moderating influence resulted in a low LST in Zone 1.

Water surfaces have the lowest daily surface temperature compared to other land covers like forests, grasslands, or urban areas during the growth season each year. This phenomenon can be attributed to differences in the heat-absorbing and heat-retaining properties of water and land (Li et al. 2020b). In this study, small site "water" (T_S6) and Zone 1, excluding the area covered by the reservoir (T_Z1_WW), had lower surface temperatures than other small sites (Fig. 9). Small sites where there were built-up areas (T_S2, T_S4, T_S5), in contrast, had higher surface temperatures than other small sites, because buildings absorb and store energy from the sun's radiation more effectively than natural surfaces (Nugroho et al. 2022). The difference in surface temperature of small site "water" (T_S6) and those where there are built-up areas (T_S2, T_S4, T_S5) was significantly higher both in August and September since 1985. In these months, the greatest increase was recorded for the permanently built-up site (T_S4; see regression coefficients in Appendix). This is mainly due to the thermal lag of water bodies (Pickens et al. 2022), which is supported by the thermal regime of the water in the Kaniv Reservoir (Vandiuk 2013).

A positive trend in surface temperature in the three zones without water or open water bodies (Z1_W, Z2_W) and six small locations throughout the entire period studied (1985–2022) was recorded (Fig. 8b, 9). Vyshnevskyi and Shecvhuk (2021) report an increase in mean water temperature in the Dnipro Cascade during summer of 0.74 °C per decade since the late 1970s. A statistically significant trend in the LST for all sites in August and September can be attributed to a natural cycle in the climate and presence of the reservoir, as air temperature is lower in spring and the first half of summer (cooling effect), then increases in the second half of summer and autumn (warming effect).

Conclusion

This study detected and quantified an increase in built-up areas in the shoreland zone of Kaniv Reservoir throughout this 37-year study (1985–2022). Surface temperature in the built-up area increased unevenly over time and differently in each of three zones studied. The zone with the biggest increase in built-up areas is located close to the city of Kyiv along the shore of the reservoir. The LST in this zone was mitigated by the presence of the reservoir. The highest LST values were recorded in the zone where agriculture dominated. Positive LST trends were recorded throughout the entire study, albeit with differences in the slopes in individual months and these were statistically significant only in August and September.

This study provides valuable insights into the thermal dynamics associated with reservoirs adjacent to urban developments. The findings increase our understanding of the multifaceted effects of large reservoirs and urbanization on regional climates, especially the variations in temperature and land cover dynamics.

Acknowledgements

This work was supported by the Ministry of Education, Youth and Sports of the Czech Republic within the CzeCOS program, grant number LM2023048; and the Ministry of Education and Science of Ukraine, Agreements Nos. M/65-2021 from 17 November 2021 and M/5-2022 from 16 May 2022. We express our gratitude for the collaboration that resulted in this study within the framework of SCERIN (The South, Central and East European Regional Information Network).

REFERENCES

Arulbalaji P, Padmalal D, Maya K (2020) Impact of urbanization and land surface temperature changes in a coastal town in Kerala. India Environ Earth Sci. doi: 101007/s12665-020-09120-1.

Bala R, Prasad R, Yadav VP (2021) Quantification of urban heat intensity with land use/land cover changes using Landsat satellite data over urban landscapes. Theor Appl Climatol. doi: 101007/s00704-021-03610-3.

Chen J, Ban Y, Li S (2014) Open access to Earth land-cover map. Nature. doi: 101038/514434c.

Chuvieco E (2016) Fundamentals of satellite remote sensing: an environmental approach. CRC Press, Boca Raton.

Cover T, Hart P (1967) Nearest neighbor pattern classification. IEEE Trans. Inf. Theory. doi: 10.1109/TIT.1967.1053964.

Dawson R, Khan MSA, Gornitz V, Lemos MF, Atkinson L, Pullen J, Osorio JC (2018) Urban areas in coastal zones. In: Rosenzweig C, Solecki W, Romero-Lankao P, Mehrotra S, Dhakal S, Ali Ibrahim S (eds) Climate change and cities: second assessment report of the urban climate change research network. Cambridge University Press, Cambridge, pp. 319–362.

Decree of Ministry of Environmental protection and natural resources of Ukraine (2022) On the approval of the Regulations on recreational activities between the territories and objects of the natural reserve fund of Ukraine, 26.07.2022 № 256. In Ukrainian.

Ermida S, Soares P, Mantas V, Göttsche F-M, Trigo IF (2020) Google Earth Engine Open-Source Code for Land Surface Temperature Estimation from the Landsat Series. Remote Sens. doi: 10.3390/rs12091471.

Gorelick N, Hancher M, Dixon M, Ilyushchenko S, Thau D, Moore R (2017) Google Earth Engine: Planetary-scale geospatial analysis for everyone. Remote Sens Environ. doi: 10.1016/j.rse.2017.06.031.

He H, Hamdi R, Cai P, Luo G, Ochege FU, Zhang M, Termonia P, De Maeyer P, Li Ch (2021) Impacts of historical land use/cover change (1980–2015) on summer climate in the Aral Sea region. J Geophys Res-Atmos. doi: 10.1029/2020JD032638.

Köppen W (1936) Das geographische System der Klimate. Gebrüder Borntraeger, Berlin.

Kurbanov NB, Kurbanov ShB (2014) Modern adaptation approach of agriculture to climate change and reservoirs impact Innovations. Agriculture 3: 5–10. In Russian.

Kussul N, Shelestov AYu, Basarab R, Yailymov B, Lavreniuk M, Kolotii A (2016) High resolution land cover for Ukraine. In: Fedorov O (ed.) Space research in Ukraine 2014–2016. Akademperiodyka, Kyiv, pp. 44–48.

Li T, Cao J, Xu M (2020a) The influence of urban spatial pattern on land surface temperature for different functional zones. Landsc Ecol Eng. doi: 101007/s11355-020-00417-8.

Li YL, Liu X, Qian F (2020b) Research on water thermal effect on surrounding environment in summer. Energy Build. doi: 101016/jenbuild2019109613.

Martazinova VF (2019) Instability of daily summer air temperature from the beginning of the XXI century at Kyiv weather station. Ukr Geogr J 3: 15–21.

Morsy M, Aboelkhair H (2021) Assessment of agricultural expansion and its impact on land surface temperature in El-Beheira Governorate, Egypt. Egypt J Remote Sens Space Sci. doi: 101016/jejrs202103003.

NASA/METI/AIST/Japan Spacesystems and US/Japan ASTER Science Team (2019) ASTER Global Digital Elevation Model V003 [Data set] NASA EOSDIS Land Processes Distributed Active Archive Center. https://doiorg/105067/ASTER/ASTGTM003. Accessed 16 August 2023.

Nugroho NY, Triyadi S, Wonorahardjo S (2022) Effect of high-rise buildings on the surrounding thermal environment. Build Environ. doi: 101016/jbuildenv2021108393.

Obodovskyi OG (2002) Deyaki aspekty doslidzhen ruslovykh protsesiv u nyzhnikh byefakh (na prykladi Dniprovs'kykh hidrovuzliv) (Some aspects of studies of channel processes below dams, for example Dnieper hydroelectric power plants). Hidrolohiya hidrokhimiya i hidro ekolohiya 4: 106–111.

Prasomsup W, Piyatadsananon P, Aunphoklang W, Boonrang A (2020) Extraction technic for built-up area classification in Landsat 8 imagery. Int J Environ Sci Dev. doi: 1018178/ijesd20201111219.

Pickens H, Hansen MC, Stehman SV, Tyukavina A, Potapov P, Zalles V, Higgins J (2022) Global seasonal dynamics of inland open water and ice. Remote Sens Environ. doi: 101016/jrse2022112963.

Roerdink J, Meijster A (2001) The watershed transform: definitions, algorithms, and parallelization strategies. Fundam Inform. doi: 10.3233/FI-2000-411207.

Starodubtsev V, Ladyka M, Bogdanets V, Naumovska L (2021) Dams and environment: landscapes change in the Kaniv reservoir on the Dnieper river, Ukraine. In: Kuprienko SV (ed.) Intellectual development of mankind in modern conditions; psychology, philology, medicine, biology and ecology. Odessa, pp. 104–125.

Tarawally M, Xu W, Hou W, Mushore TD (2018) Comparative analysis of responses of land surface temperature to long-term land use/cover changes between a coastal and inland city: a case of Freetown and Bo town in Sierra Leone. Remote Sens. doi: 103390/rs10010112.

Timonina M (2020) Resident population of Ukraine by sex and age on January 1, 2020. State Statistics Service of Ukraine, Kyiv.

Trlica A, Hutyra LR, Schaaf CL, Erb A, Wang JA (2017) Albedo, landcover, and daytime surface temperature variation across an urbanized landscape. Earth Future. doi: 101002/2017EF000569.

Vandiuk NS (2013) Thermal regime of the Kaniv Reservoir as one of important factors of functioning of its ecosystem. Hydrobiol J. doi: 101615/HydrobJv49i690.

Vendrov SL, Avakyan AB, Dyakonov KN, Reteum AY (1968) The role of reservoirs in changing natural conditions. Knowledge, Moscow. In Russian.

Vyshnevskyi V, Shecvhuk S (2021) Thermal regime of the Dnipro Reservoirs. J. Hydrol. Hydromech. doi: 10.2478/johh-2021-0016.

Vyshnevskyi VI, Stashuk VA, Sakevych AM (2011) Water management complex in the Dnieper basin. Interpres LTD, Kyiv. In Ukrainian.

Appendix

Table 4 Regressions and regression coefficients for surface temperature trend during the period of 37 years for individual months from May to September. Information is presented for six small sites (T_S1–T_S6), conditional Zone 1 (T_Z1), conditional Zone 1 with reservoir water area (T_Z1_W), conditional Zone 1 without reservoir water area (T_Z1_WW), and air temperatures for Kyiv (T_AIR_KY_9.30). This information complements the graphs in Fig. 9 of the main text.

Month	Regression coefficients	Month	Regression coefficients
May	T_S1 = 20.33 + 0.0002 × x; T_S2 = 19.63 + 0.0002 × x; T_S3 = 9.72 + 0.0003 × x; T_S4 = 18.77 + 0.0003 × x; T_S5 = 14.73 + 0.0004 × x; T_S6 = 7.30 + 0.0002 × x; T_Z1_W = 7.35 + 0.0002 × x; T_Z1_WW = 9.47 + 0.0004 × x. T_AIR_KY_9.30 = 9.75 + 0.0003 × x	June	T_S1 = 36.50-0.0002 × x; T_S2 = 25.88 + 0.0001 × x; T_S3 = 24.21 + 3.6173E-5 × x; T_S4 = 26.28 + 0.0002 × x; T_S5 = 23.76 + 0.0002 × x; T_S6 = 17.34 + 0.0001 × x; T_Z1_W = 17.70 + 0.0001 × x; T_Z1_WW = 22.30 + 0.0002 × x; T_AIR_KY_9.30 = 22.36 + 0.00006 × x
July	T_S1 = 25.52 + 0.00008 × x; T_S2 = 21.70 + 0.0002 × x; T_S3 = 12.27 + 0.0003 × x; T_S4 = 13.84 + 0.0005 × x; T_S5 = 27.53 + 0.0001 × x; T_S6 = 10.57 + 0.0003 × x; T_Z1_W = 10.85 + 0.0003 × x; T_Z1_WW = 18.17 + 0.0003 × x; T_AIR_KY_9.30 = 20.17 + 0.0001 × x	August	T_S1 = 19.98 + 0.0003 × x; T_S2 = 11.84 + 0.0005 × x; T_S3 = 7.10 + 0.0005 × x; T_S4 = 4.97 + 0.0007 × x; T_S5 = 10.47 + 0.0005 × x; T_S6 = 6.11 + 0.0004 × x; T_Z1_W = 6.40 + 0.0004 × x; T_Z1_WW = 9.85 + 0.0005 × x; T_AIR_KY_9.30 = 8.98 + 0.0004 × x
September	T_S1 = 0.20 + 0.0006 × x; T_S2 = -0.23 + 0.0006 × x; T_S3 = -3.30 + 0.0006 × x; T_S4 = -7.88 + 0.0008 × x; T_S5 = -4.04 + 0.0007 × x; T_S6 = -3.01 + 0.0005 × x; T_Z1_W = -2.50 + 0.0005 × x; T_Z1_WW = -3.73 + 0.0007 × x; T_AIR_KY_9.30 = 2.97 + 0.0004 × x		